Achieving superlubricity of ricinoleic acid in the steel/Si3N4 contact under boundary lubrication

Yun Long (longyun0225@gmail.com)
Ecole Centrale de Lyon
Jean Michel Martin
École Centrale de Lyon: Ecole Centrale de Lyon
Frederic Dubreuil
École Centrale de Lyon: Ecole Centrale de Lyon
Maria-Isabel De Barros Bouchet
École Centrale de Lyon: Ecole Centrale de Lyon

Research Article

Keywords: OH functional group, unsaturated fatty acid, boundary lubrication, Superlubricity

Posted Date: June 13th, 2022

DOI: https://doi.org/10.21203/rs.3.rs-1718599/v1

Abstract

To improve fuel efficiency and minimize environmental pollution, the interest in organic friction modifiers has resurged, especially fatty acids. Efforts have been made to enhance fatty acids' performance by tuning their saturation state and adding OH lateral groups in the alkyl chain. Here we compared lubrication properties in the boundary regime for oleic acid (OA), ricinoleic acid (RA), and linoleic acid (LA) under the same viscosity for a steel/Si_3N_4 tribopair. The presence of the OH group in the OA chain reduces not only friction coefficient (CoF) by ~ 70% but also prevents scratches from generating on both surfaces. In the meantime, it determines local friction distribution by controlling top surface terminations. Even at 100°C, the steady-state friction coefficient of steel/Si_3N_4 lubricated by RA is only 0.014. A temperature decrease to 80°C leads to a superlubricity regime (CoF < 0.01) resulting from the cooperation of nanometer-thick liquid film (possibly containing water) and low friction of contact asperities terminated by OH hydroxyl groups provided by RA. In summary, steel/Si_3N_4 contact lubricated by ricinoleic acid gives unsurpassed tribological performances reaching superlubricity under a wide range of operating conditions.

1. Introduction

On the path towards less energy consumption and greenhouse gas emission, the fuel consumption of mechanical systems is required to be further decreased. This objective encourages researchers to cut down energy costs with low viscosity lubricants as shearing viscous ones consume great energy. However, low viscosity lubricants result in more asperities being in contact due to their poor ability on liquid film formation. Therefore, molybdenum-based friction modifier (FM), nanoparticles, organic FM, etc. [1] must be added to lubricants. Only organic FMs are studied in this work since most of them contain solely light elements like C, H, O, and N [2] and are eco-friendly.

Among organic FM, fatty acids are extensively investigated as they possess both polar group and alkyl chain, giving them an amphiphilic nature. Their polar acid group bridges fatty acid with the surface by chemical or physical adsorption [3], and acid groups were more efficient than OH, NH_2, and CN groups [4]. Fatty acid adsorption on the substrate is detected by both polarization microscopy [5] and atomic force microscopy (AFM) [6]. Concerning steel [7], silicon nitride [8] silicon carbide [9], close-packed fatty acids root on surfaces and support the charge, which avoids direct contact between surfaces [10].

The lubricity of fatty acid is influenced by alkyl chain length. Significant friction reduction starts to be recorded when six carbon atoms are present in the alkyl chain [9]. When chain length is fixed at 18 carbon atoms, in general, the unsaturation of the alkyl chain disturbs the organization of fatty acid chains on the surface to form a close-packed layer and is accompanied by friction rise [3]. Therefore, in PAO 4 base oil, the lubricity of stearic acid (SA) as an additive is better than oleic acid (OA) and linoleic acid (LA) at 150°C [3]. Nevertheless, this tendency doesn't apply to them as additives in fuel oil, where LA outperforms OA and SA with the formation of a cross-linked insulating film on steel [11].

On the other hand, unsaturated fatty acids can also contribute to the aromatization of diamond-like carbon (a-C) top surfaces. They can achieve superlubricity thanks to their function groups, which crosslink on surfaces resulting in molecule decomposition under shearing [12]. From our previous works on asymmetric tribo-pairs (Fig. 1): steel/a-C [13] and a-C/Si_3N_4 [14], contacts show superlubricity under lubrication by both ricinoleic acid (RA), and this has been attributed to the formation of hydrocarbon oligomers on a sp^2 carbon enriched a-C surface. Additionally, from the simulation of the a-C/Si_3N_4 shearing process, RA molecules experience a cascade decomposition, resulting in small hydrocarbon oligomers forming on the a-C surface. It is worth mentioning that for steel/a-C and a-C/Si_3N_4 pairs, the lubrication of OA leads to a slight increase in CoF, which exceeds the superlubricity range compared to RA lubrication cases (Fig. 1). However, LA lubricating steel/a-C causes the highest CoF-0.055 among those three fatty acids.

In this paper, the tribological performances of RA, OA, and LA are further investigated using the steel/Si_3N_4 tribopair in the absence of the a-C coating, thus enlarging the application range of unsaturated fatty acids studied in our previous works [13, 14]. The objective here is twice: (i) achieving or not superlubricity in the absence of carbon material a-C coating lubricated by the different fatty acids and (ii) identifying the role of the number of doubles bonds and the presence of the OH lateral group in the alkyl chain of RA.

Worn surfaces are analyzed by combining scanning electron microscopy (SEM)/energy-dispersive X-ray spectroscopy (EDS), Raman, X-ray photoelectron spectroscopy (XPS), and AFM. Afterward, the mechanism to achieve superlubricity in the presence of RA is discussed.

2. Material And Methods

2.1. Materials

AISI 52100 steel pins and Si_3N_4 discs were purchased from Rocholl GmbH (Eschelbronn, Germany) and LianYunGang HighBorn Technology (LianYunGang, China), respectively. Rocholl GmbH processed steel pins with a 100 mm radius spherical top and a roughness of 5.5 nm. Their elastic modulus (E) is 210 GPa, and Poisson Ratio (v) is 0.3. Si_3N_4 discs with E, v as 310 GPa, 0.27 were manufactured by hot pressing.

Three lubricants: (RA) ricinoleic acid (purity ≥99%), (LA) linoleic acid (purity ≥99%), and (OA) oleic acid (purity ≥99%) are chosen to study the impact of C=C and C-OH bonds in the alkyl chain on the tribological performances. All additives are provided by Sigma-Aldrich (St. Louis, USA), with molecular structures shown in Fig. 1.

2.2. Tribological experiments

Before the friction test, samples were first cleaned in n-heptane and then in acetone for 30 min and 5 min, respectively. Afterward, steel pins and Si_3N_4 discs were installed on a linear reciprocating tribometer described in previous work [15], and ~ 50 µL of lubricant was added to the contact zone. A sine function controls the movement of this tribometer, and sliding speed is noted at its highest value during the tribometer motion, *i.e.*, three mm/s in our case. The normal force is applied vertically on the disc and is fixed at 70N, corresponding to a Hertzian contact diameter of 680 mm and initial contact pressure of around 200 MPa. Four temperatures, 50°C, 60°C, 80°C, and 100°C, were considered in this study.

2.3. Analysis of worn surfaces

Worn surfaces were first washed with ethanol, then with n-heptane. They were later imaged by digital microscopy (VHX-6000, Keyence, Osaka, Japan) and interferometry (ContourGT-K1, Bruker, Billerica, USA) to visualize and quantify wear volumes. Interferometry was also used to obtain surface roughness (Sa) by calculating height distribution on a 126 x 95 μm^2 large area.

Considering that SEM/EDS and Raman analyses may cause irradiation damage to surface chemistry, XPS was first performed on samples with a ULVAC-PHI Versa Probe II spectrometer, using an Al Kα X-ray source. C1s and O1s spectra were collected by analyzing an area of 200 x 200 µm² at a take-off angle of 45 ° and a pass energy of 23.5 eV. Afterward, spectra were fitted by Multipack software and calibrated by indexing the FeOx peak in O1s to 530.0 eV binding energy (BE) [16].

Samples were later analyzed by SEM/EDS (MIRA3 FEG, Tescan, Brno - Kohoutovice, Czech Republic). The electron beam was accelerated at 5 KeV for SEM imaging and EDS analysis. SEM images were taken in secondary electron mode. For EDS analysis, working distance and dead time were kept at 15 mm and 30%, respectively.

Raman analysis was performed by Invia^{TM} Raman spectrometer from Renishaw (UK), operating with a 633 nm laser. The laser power was limited to 10 mW to avoid surface damage.

An atomic force microscope (Park NX, Park systems, Suwon, South Korea) is used to investigate samples' topographic information and quantify the lateral force between silicon tip and surfaces by operating in contact mode. AFM tips are bought from Bruker (RESP-20 with cantilever length of 450 mm, width of 50 mm, and k= 0.9 N/m).

3. Experimental Results

3.1. Influence of nature of fatty acid on friction

From Fig. 1, RA and OA have similar molecular structures, but RA has one OH lateral group branched on the aliphatic chain. RA and OA have only one C=C bond, but LA has twice. Consequently, the presence of a hydroxyl group in the chain of RA provokes a significant increase in viscosity at a given temperature. To avoid viscosity changes on tribological performance and focus only on tribo-chemical reactions between

lubricants and surfaces, friction tests are conducted with the same viscosity for the three lubricants, fixed at 11 mPa.s^{-1} [17,18]. This is obtained by operating at three different temperatures for OA, LA, and RA, which are 60°C, 50°C, and 100°C, respectively. Each test is performed three times to study the reproducibility.

Under iso-viscous lubrication of fatty acids, friction behaviors of steel/Si_3N_4 tribo-pairs are determined by the fatty acid type (Fig. 2a). The lubrication by OA stabilizes with a friction coefficient (CoF) near 0.05. The friction curves for the LA case show a continuous decrease of CoF with sliding time, ending at ~ 0.06 after 1.1 hours of sliding. Concerning the RA lubrication case, CoF stabilizes near 0.014 at the end after a long running-in period, approaching superlubricity. Remarkable differences are also observed in wear scars. 3D depth profiles of steel pins lubricated by RA (Fig. 2j) display shallow scratches with a height of less than 15 nm, and those scratches aren't visible in the corresponding optical image (Fig. 2c). Meanwhile, the wear scar on steel is slightly polished with values from 5.5 nm (Sa of virgin steel) to 4.9 nm. Scratches are also detected on steel pins lubricated by OA (Fig. 2b, i, h) and LA (Fig. 2d, k), but their depth is greater than in the RA lubrication case. Correspondingly, in their 3D depth profiles, dark blue (Fig. 2i, k) and even black straight lines (Fig. 2h) are observed inside wear scar. On Si_3N_4 discs, no detectable wear scars are recorded for RA, and LA lubrication cases (Fig. 2f, g), and only one black scratch is found on the Si_3N_4 disc after OA lubrication (Fig. 2e).

To conclude on this set of tests with steel/Si_3N_4 contact, we observed that superlubricity is not achieved at 100 °C by the three unsaturated fatty acids, which is inconsistent with the case for the DLC-containing tribo-pairs (Fig. 1). Among them, RA is the best lubricant, with a CoF approaching 0.01.

SEM/EDS analyses were performed on steel pins to visualize wear scars and acquire chemical information. For the RA lubrication case, the wear scar on the steel pin is homogenous (Fig. 3b), with only carbon (C), oxygen (O), iron (Fe), and a negligible amount of silicon (Si) detected by EDS (Fig. 3f) like these analysis results outside wear scar (Fig. 3d, h). However, LA lubrication leaves steel pins with particles formed inside wear scar, which appear dark grey in the SEM image (Fig. 3c). EDS analysis on those particles shows a more substantial contribution of Si and O elements (Fig. 3g) than outside. On the other hand, OA lubrication leaves a large groove inside the steel pin (Fig. 3a), containing black wear particles. Their EDS analysis shows remarkable Si and Nitrogen (N) contents, indicating Si_3N_4 derived materials being transferred from Si_3N_4 disc to steel pin.

Raman analysis unveils wear debris structures (Fig. 4). For the OA lubrication case, hematite a-Fe_2O_3 [19] is detected on steel pins thanks to four characteristic peaks recorded at 222, 289, 408, and 1315 cm^{-1}. A peak at 672 cm^{-1} [20] suggests that magnetite Fe_3O_4 is also present in wear particles. Besides, the peak at 1586 cm^{-1} corresponds to carbon with sp^2 hybridization [21], also known as the carbon G peak. Another peak recorded at 620 cm^{-1} is attributed to the Si-O bond [22] even though the E_{2g} mode of β-Si_3N_4 [23] is also located at 620 cm^{-1}. Other characteristic peaks of β-Si_3N_4 are not observed in Fig.4. Combining Raman and EDS analysis, we conclude that wear particles formed after OA lubrication consist of iron

oxides and carbon/silicon-based materials. Otherwise, LA lubrication generates wear particles composed of hematite and magnetite on steel pins. Interestingly, no wear particles are formed on steel pins lubricated by RA, and the Raman signal is that of steel substrate outside wear scar.

XPS further identifies the chemical change of the steel worn surface in Figure 5. However, XPS analyses on the ceramic side could not be carried out in the three cases because the wear scar could not be optically detected in the UHV chamber. From XPS survey spectra, elements C, O, Fe and Si are detected on all surfaces, but Si content remains as low as 0.4 at% regardless of probed areas present in the steel composition. For example, a high-resolution XPS was performed on the steel pin close to the violet mark shown in Fig. 2b in the OA lubrication case. After fixing the O1s peak of iron oxide at 530.0 eV BE for calibration, the C1s peak is first discussed (Fig. 5a-c) for the three acids. C-O, C=O, and O-C=O bonds are detected at 286.3, ~287.5, and 288.7 eV BE, respectively, for the three tests (SI Table 1) in agreement with data in the literature. The location of O-C=O at 288.7 eV BE in all cases indicates the presence of iron carboxylate (COOFe) because the corresponding acid COOH bond has binding energy ≥289.2 eV [3]. This demonstrates that acids have reacted chemically with iron oxides.

Concerning the O1s spectra, a FeOOH (hydroxide species) peak is found at 531.4 eV BE naturally present on steel surfaces. In addition, O=C and O-C peaks are also observed at 532.2 and ~533.1 eV BE, respectively. But they also contain O=C, O-C signals originating from carboxylates (-C(O)O-) groups. In the case of LA, the increase in carboxylate species at the C1s peak is correlated with the corresponding increase of intensity of the O=C-O contribution in the O 1s peak. Furthermore, water located at 534.3 eV is observed on steel surface lubricated by RA and LA, and it is not for the OA lubrication case. Water can either derive from humid air or/and tribo-chemical reaction driven by shearing.

To conclude on XPS analysis of steel pins, the three unsaturated fatty acids (or their derivatives) are strongly chemisorbed on iron oxide/hydroxides by forming iron carboxylate and a very thin layer (< 5nm) is formed on iron oxides as detected by XPS. RA lubrication shows the highest C-O bond contribution on steel surfaces compared to the other unsaturated fatty acids. In a previous paper [14], we demonstrated by computer simulation that RA molecules are entirely broken when they are sheared in a DLC/Si_3N_4 asperity contact. It is plausible that similar tribochemical reactions could occur in the present case even though the hardness of the steel is lower than that of the DLC, primarily since steel can act as a catalyst in the decomposition of specific molecules. Eventually, AFM analyses are performed on steel surfaces after friction tests. It is worthy to note that AFM analyses were conducted on the same day with the same conditions (single tip, no change in laser position), allowing comparison between the three cases. On a scale of 3.5×3.5 mm², scratches are found on surfaces lubricated by OA and LA with a depth larger than 5 nm, while the depth of scratch of steel lubricated by LA could reach ~13 nm (Fig. 6g). On the other hand, scratches are also observed on surfaces lubricated by RA, but most of them have a depth of ~3 nm, and they align along the sliding direction (Fig. 6d-f). Despite the topography changes between surfaces lubricated by OA, and LA (Fig. 6a, c), their corresponding friction forces are similar and equal to 0.04 ± 0.005 mV (Fig. 6h). The friction force is calculated by averaging the lateral force signal difference

between back and forward traces. Intriguingly, the friction force of steel surface lubricated by RA strongly depends on the position of analyses and is not homogeneously distributed (Fig. 6b).

There are zones with a friction force of ~ 0.23 mV (Fig. 6h), nearly half of the signal measured in other places, including OA and LA lubrication cases. The locations of low friction patches (Fig. 6b) on a steel surface lubricated by RA correlate with a tiny topography change, not greater than 2 nm (Fig. 6e, g). It has already been shown that AFM can easily detect monolayers of organic acids on ultra-smooth surfaces [6]. Of course, the situation is different on steel because of the inherent roughness of such substrates. However, we can say that the thicknesses of low-friction patches are not above 2-3 nm.

Due to the formation of carboxylate bonds, unsaturated fatty acids can firmly attach to the steel surface [3]. Considering the molecular structures of OA, RA, and LA (Fig.1), OA and LA's attachment on steel surfaces enables top surfaces with CH_3 termination. In contrast, the chemisorption of RA on steel surfaces can create either CH_3 or OH terminations. Compared with contact between two CH_3-terminated surfaces, OH-terminated surfaces generally show lower adhesion force [24] and lower lateral force [25]. Therefore, low friction patches are attributed to OH-containing species on the surface. This agrees with the steel surface lubricated by RA, which has the most substantial C-OH contribution in XPS analysis (Fig. 5).

3.2. Achieving superlubricity with ricinoleic acid

Regarding the most interesting RA lubrication case, Figure 7 shows that CoF is further reduced and reduced when lowering the testing temperature to 60°C. Superlubricity can be achieved with the smallest CoF of 0.003 realized at 60°C. On the other side, the temperature decrease does not change significantly steel wear scar diameters and radius of curvature, which is quite similar to the original curvature of the ball, i.e., 100 mm (table 1). The curves in Fig 7a have been calculated using the friction values averaged near the track center, corresponding to sliding speeds between 2.5 mm/s and 3 mm/s. By processing the last 20 cycles of the test, the evolution of CoF against sliding speed in the three cases is more interesting (Fig 7b). Friction curves at 60°C and 80°C show much lower CoF than those at 100°C, but including extremities of the wear track where the speed changes in direction. Therefore, we conclude that superlubricity has been achieved at these two temperatures even under severe boundary lubrication conditions (very low speeds).

4. Discussion

Starting with the role of the hydroxyl group added to monounsaturated fatty acid (OA case), the adding OH function in the aliphatic chain (RA case) raises lubricant viscosity by establishing hydrogen bonds between molecules [17, 18]. On the contrary, adding a second C=C function group (LA case) reduces lubricant viscosity by increasing possible molecular conformations. Besides their influence on viscosity, OH function groups also determine the tribological performance of the steel/Si_3N_4 pair (Fig. 2). For instance, the lowest CoF is obtained by RA lubrication but not OA and LA for steel/Si_3N_4 contact at iso-

viscosity conditions. The presence of the OH group on unsaturated fatty acid chains prevents internal material exchange between Si_3N_4 and steel (Fig. 3). It also limits iron oxides type wear particles formation on steel (Fig. 4) and augmentation of surface roughness. XPS data (Fig. 5) show steel surface lubricated by RA has a more significant C-O content than LA and OA lubrication cases. Meanwhile, only steel pin lubricated by RA is covered with low friction patches (Fig. 6), attributed to OH containing species formation on the surface. Indeed, OH lubrication limits energy dissipation by reducing friction [26]. This explains why RA overrides the lubricity of OA and LA at the same viscosity (Fig.2).

Table 1. Detailed information on steel/Si_3N_4 lubricated by RA under different temperatures. It contains the diameter of wear (D_w), Hertzian contact diameter (D_H), average contact pressure (P_{ave}), the radius of curvature inside the wear scar (R_w), and calculated liquid film thickness (h_c), and lambda value. This Table was previously reported in Long. Y's Ph.D. thesis [27].

	RA-60°C		RA-80°C		RA-100°C	
Viscosity (mPa·s)	42.0 [17]		24.8 [17]		11.1	
CoF at 1.1h	0.003		0.005		0.014	
	Pin	Flat	Pin	Flat	Pin	Flat
D_w (mm)	716	-	788	-	810	-
D_H (mm)	678	-	678	-	678	-
P_{ave} (MPa)	176		146		138	
R_w (mm)	102.7	-	106.4	-	112.1	-
Sa before the test (nm)	5.5	12.4	5.5	12.4	5.5	12.4
Sa after the test (nm)	6.2	12.4	5.5	12.4	4.9	12.4
h_c (nm)	8.8		6.2		3.7	
Lambda	0.63		0.48		0.27	

By decreasing the temperature from 100°C to 80°C, superlubricity can easily be obtained for steel/Si_3N_4 pairs lubricated by RA (Fig. 7). Since the testing temperature does play a role in friction behavior, surfaces may partially be separated by a thin liquid film. The lambda ratios stay below unity regardless of testing temperatures. A continuous liquid film is not expected to form between the overall contacting surfaces. In the state of our knowledge, clear evidence of superlubricity under severe boundary lubrication conditions (lambda <1) has not been shown before. Furthermore, it is questionable if EHL film thickness calculation can be reasonably applied to a molecular liquid film (inferior to 5 nm). Due to the lack of a complete

liquid film to separate surface contact, creating an easy-shear contact between asperities is also crucial to minimize friction. Derived from the attachment of fatty acids on surfaces, the contact between methyl groups on fatty acids reduces friction by avoiding metal contacts [1]. Still, CoF below 0.05 is hardly attainable at the macroscale [3]. However, friction between asperities can be further decreased by introducing the OH group in the alkyl chain of fatty acids, resulting in low friction patches forming on surfaces (Fig. 6). The origin of water found by XPS on the worn surface needs more investigation to know if it can contribute to lower friction, and computer simulations are currently under investigation.

5. Conclusion

The lubrication capabilities of RA, OA, and LA have been evaluated in a steel/Si_3N_4 tribo-pair under boundary lubrication conditions. The results are compared with those from other friction pairs involving a-C material (a-C/Si_3N_4 and steel/a-C) that have been previously published. Under iso-viscous conditions, the CoF of RA lubrication is ~ 30% lower than the two other cases and approaches a superlubricity regime at 100°C. Correspondingly, the wear scar on the steel pin is polished by RA lubrication, while OA and LA cases leave steel pins with deep scratches and wear particles formation. The unique OH lateral group on the alkyl chain distinguishes RA from other fatty acids as it governs friction by generating nanometer-thick low friction patches. Moreover, superlubricity is realized when the temperature is ≤ 80°C, a reasonable temperature for industrial applications. Superlubricity at three mm/s can be explained by the cooperation of OH terminated patches with a partial nanometer-thick fluid film in other parts. However, results show that superlubricity is conserved even if sliding speeds are under 0.5 mm/s, corresponding to film thickness calculation below 1 nm so that any fluid film is practically absent. The role of water molecules possibly generated inside the interface zone may be involved in the mechanism.

Declarations

The authors declare that there is no competing financial interest.

Acknowledgments

Centre de Recherche de Solaize (CReS) of TotalEnergies, France, supported this research.

References

1. *Spikes, H.: Friction modifier additives. Tribol. Lett. 60, 1-26 (2015). https://doi.org/10.1007/s11249-015-0589-z.*
2. *Ewen, J.P., Gattinoni, C., Morgan, N., Spikes, H.A., Dini, D.: Nonequilibrium molecular dynamics simulations of organic friction modifiers adsorbed on iron oxide surfaces. Langmuir 32, 4450-4463 (2016). https://doi.org/10.1021/acs.langmuir.6b00586.*
3. *Loehlé, S., Matta, C., Minfray, C., Le Mogne, T., Iovine, R., Obara, Y., Miyamoto, A., Martin, J.M.: Mixed lubrication of steel by C18 fatty acids revisited. Part II: Influence of some key parameters. Tribol. Int.*

94, 207-216 (2016). https://doi.org/10.1016/j.triboint.2015.08.036.

4. *Jahanmir, S., Beltzer, M.: Effect of additive molecular structure on friction coefficient and adsorption. J. Tribol. 108, 109-116 (1986). https://doi.org/10.1115/1.3261129.*
5. *Tadokoro, C., Araya, S., Okubo, H., Nakano, K., Sasaki, S.: Polarization observations of adsorption behavior of fatty acids using optical anisotropy of liquid crystal. Tribol. Lett. 64, 1-9 (2016). https://doi.org/10.1007/s11249-016-0765-9.*
6. *Salmeron, M.: Generation of defects in model lubricant monolayers and their contribution to energy dissipation in friction. Tribol. Lett. 10, 69-79 (2001). https://doi.org/10.1023/A:1009026312732.*
7. *Lundgren, S.M., Persson, K., Mueller, G., Kronberg, B., Clarke, J., Chtaib, M., Claesson, P.M.: Unsaturated fatty acids in alkane solution: adsorption to steel surfaces. Langmuir 23, 10598-10602 (2007). https://doi.org/10.1021/la700909v.*
8. *Hibi, Y., Nakano, M.: Effect of Oleic Acid on Friction and Wear Behavior of Silicon Nitride in Ethanol and in n-Undecane. J. Jpn. Soc. Tribologis. 59, 515-520 (2014). https://doi.org/10.14886/sssj2008.33.0_219.*
9. *Studt, P.: Boundary lubrication: adsorption of oil additives on steel and ceramic surfaces and its influence on friction and wear. Tribol. Int. 22, 111-119 (1989). https://doi.org/10.1016/0301-679X(89)90171-0.*
10. *Salem, L.: Attractive forces between long saturated chains at short distances. J. Chem. Phys. 37, 2100–2113 (1962). https://doi.org/10.1063/1.1733431.*
11. *Martin, J.M., Matta, C., Bouchet, M.I.D.B., Forest, C., Le Mogne, T., Dubois, T., Mazarin, M.: Mechanism of friction reduction of unsaturated fatty acids as additives in diesel fuels. Friction 1, 252-258 (2013). https://doi.org/10.1007/s40544-013-0022-2.*
12. *Kuwahara, T., Romero, P.A., Makowski, S., Weihnacht, V., Moras, G., Moseler, M.: Mechano-chemical decomposition of organic friction modifiers with multiple reactive centres induces superlubricity of ta-C. Nat. Commun. 10, 1-11 (2019). https://doi.org/10.1038/s41467-018-08042-8.*
13. *Long, Y., Galipaud, J., Weihnacht, V., Makowski, S., Martin, J.M., Bouchet, M.I.D.B.: Achieving superlubricity using selected tribo-pairs lubricated by castor oil and unsaturated fatty acids, Tribo. Int. 169, 107462 (2022). https://doi.org/10.1016/j.triboint.2022.107462.*
14. *Long, Y., Wang, Y., Weihnacht, V., Makowski, S., Kubo, M., Martin, J.M., Bouchet, M.I.D.B.: Mechanism of superlubricity of a DLC/Si3N4 contact in the presence of castor oil and other green lubricants. Friction 1-14 (2022). https://doi.org/10.1007/s40544-022-0601-1.*
15. *Salinas Ruiz, V.R., Kuwahara, T., Galipaud, J., Masenelli-Varlot, K., Hassine, M.B., Héau, C., Stoll, M., Mayrhofer, L., Moras, G., Martin, J.M., Moseler, M., Bouchet, M.I.D.B.: Interplay of mechanics and chemistry governs wear of diamond-like carbon coatings interacting with ZDDP-additivated lubricants. Nat. Commun. 12, 1-15 (2021). https://doi.org/10.1038/s41467-021-24766-6.*
16. *Hadnadjev, M., Vulic, T., Marinkovic-Neducin, R., Suchorski, Y., Weiss, H.: The iron oxidation state in Mg–Al–Fe mixed oxides derived from layered double hydroxides: an XPS study. Appl. Surf. Sci. 254, 4297-4302 (2008). https://doi.org/10.1016/j.apsusc.2008.01.063.*

17. *André, E., Vernier, C.: Some Physical Properties of Pure Ricinoleic Acid: The Refractive Index, Specific Gravity, and Viscosity. J. Rheol. 3, 336-340 (1932). https://doi.org/10.1122/1.2116497.*
18. *Rabelo, J., Batista, E., Cavaleri, F.V.W., Meirelles, A.J.: Viscosity prediction for fatty systems. J. Am. Oil. Chem. Soc. 77, 1255-1262 (2000). https://doi.org/10.1007/s11746-000-0197-z.*
19. *Bersani, D., Lottici, P.P., Montenero, A.: Micro-Raman investigation of iron oxide films and powders produced by sol-gel syntheses. J. Raman Spectrosc. 30, 355-360 (1999). https://doi.org/10.1002/(SICI)1097-4555(199905)30:5<355::AID-JRS398>3.0.CO;2-C.*
20. *Shebanova, O.N., Lazor, P.: Raman study of magnetite (Fe3O4): laser-induced thermal effects and oxidation. J. Raman Spectrosc. 34, 845-852 (2003). https://doi.org/10.1002/jrs.1056.*
21. *Ferrari, A.C.: Raman spectroscopy of graphene and graphite: Disorder, electron– phonon coupling, doping and nonadiabatic effects. Solid State Commun. 143, 47-57 (2007). https://doi.org/10.1016/j.ssc.2007.03.052.*
22. *Lukianova, O.A., Parkhomenko, A.A., Krasilnikov, V.V., Khmara, A.N., Kuzmenko, A.P.: New method of free silicon determination in pressureless sintered silicon nitride by Raman spectroscopy and XRD. Ceram. Int. 45, 14338-14346 (2019). https://doi.org/10.1016/j.ceramint.2019.04.148.*
23. *Zanocco, M., Marin, E., Boschetto, F., Adachi, T., Yamamoto, T., Kanamura, N., Zhu, W., McEntire, B.J., Bal, S.B., Ashida, R., Mazda, O., Pezzotti, G.: Surface functionalization of polyethylene by silicon nitride laser cladding. Appl. Sci. 10, 2612 (2020). https://doi.org/10.3390/app10072612.*
24. *Vezenov, D.V., Noy, A., Rozsnyai, L.F., Lieber, C.M.: Force titrations and ionization state sensitive imaging of functional groups in aqueous solutions by chemical force microscopy. J. Am. Chem. Soc. 119, 2006-2015 (1997). https://doi.org/10.1021/ja963375m.*
25. *Israelachvili, J.N., Chen, Y.L., Yoshizawa, H.: Relationship between adhesion and friction forces. J. Adhes. Sci. Technol. 8, 1231-1249 (1994). https://doi.org/10.1163/156856194X00582.*
26. *Wang, Y., Hayashi, K., Ootani, Y., Bai, S., Shimazaki, T., Higuchi, Y., Ozawa, N., Adachi, K., Bouchet, M.I.D.B., Martin, J.M., Kubo, M.: Role of OH Termination in Mitigating Friction of Diamond-like Carbon under High Load: A Joint Simulation and Experimental Study. Langmuir 37, 6292-6300 (2021). https://doi.org/10.1021/acs.langmuir.1c00727.*
27. *Long, Y.: Green superlubricity mechanisms of OH-containing lubricants for hard carbon and Si-based materials. Doctoral dissertation, Lyon (2020).*

Figures

Lubricant	RA	OA	LA
Steady-state CoF for Steel/a-C(30) [13]	0.008	0.011	0.055
Steady-state CoF for a-C(30)/Si_3N_4 [14]	0.010	0.012	-
Steady-state CoF for Steel/Si_3N_4	**?**	**?**	**?**

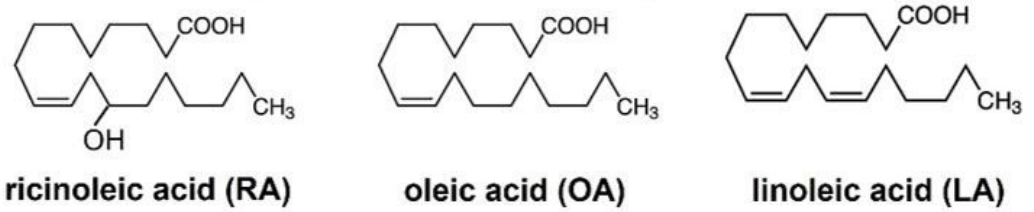

ricinoleic acid (RA) **oleic acid (OA)** **linoleic acid (LA)**

Figure 1

Molecular structures of LA, OA, and RA. Table upon molecular structures is steady-state CoF achieved in different contact configurations involving a-C(30); the value in the bracket is its hardness. All tests were performed at 100°C under boundary conditions [13, 14].

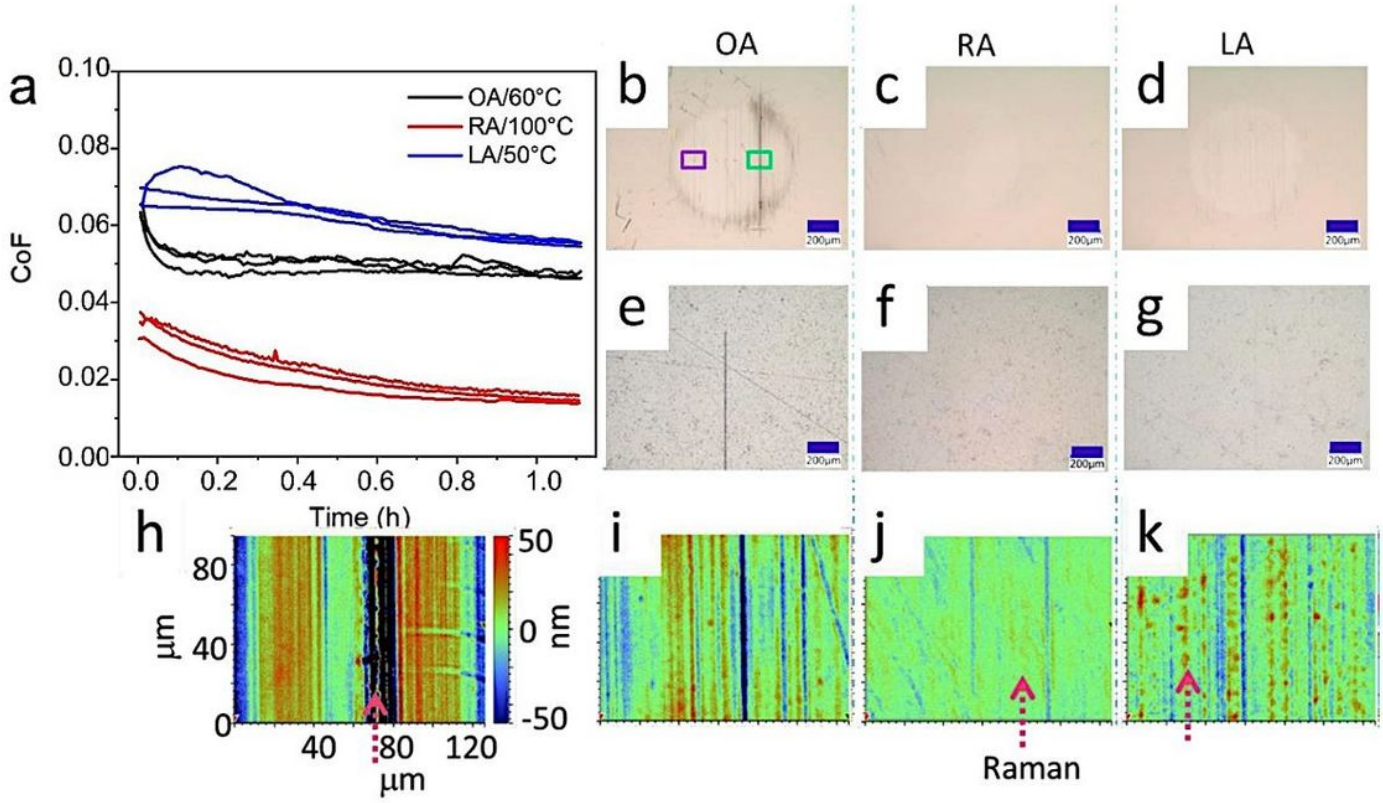

Figure 2

a Correlation between friction and time when OA, RA, and LA lubricate steel/Si_3N_4 tribo-pair under iso-viscous conditions (3 consecutive tests for reproducibility). For the case of OA lubrication, wear scars on **b** steel, **e** Si_3N_4 are visualized on optical images. Topographical information on steel is demonstrated by 3D depth profiles, where **i** corresponds to an area in a purple rectangle while **h** refers to the green zone. This arrangement of optical images and 3D depth profiles is also adopted by **c**, **f**, **j** in the case of RA lubrication and **d**, **g**, **k** in the case of LA lubrication. Red arrows in h, j, k correspond to Raman analysis spots.

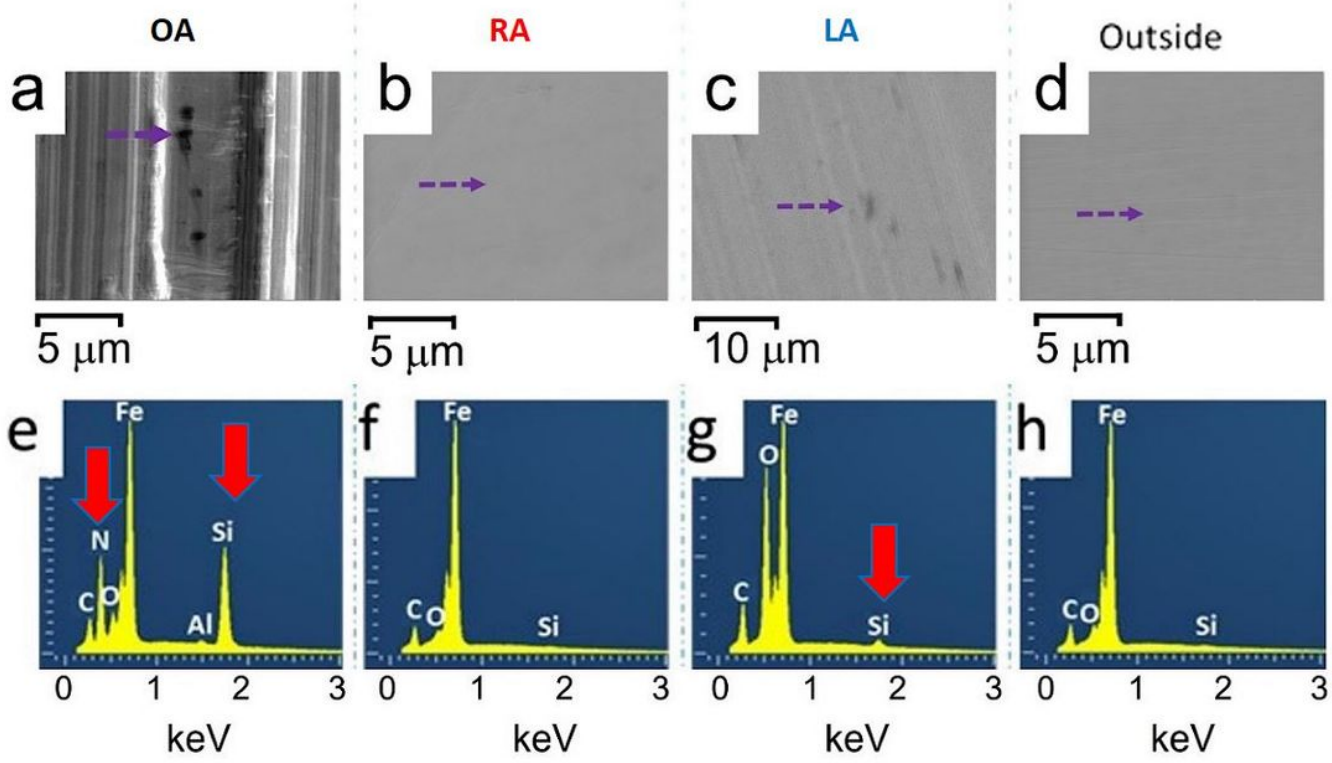

Figure 3

a-d SEM images on steel pins **d** outside wear scar, after lubrication by **a** OA, **b** RA and **c** LA inside wear scar. **e-h** EDS spectra in **h** outside wear scar, after lubrication of **e** OA, **f** RA and **g** LA. EDS analyses are performed on those spots marked by violet arrows.

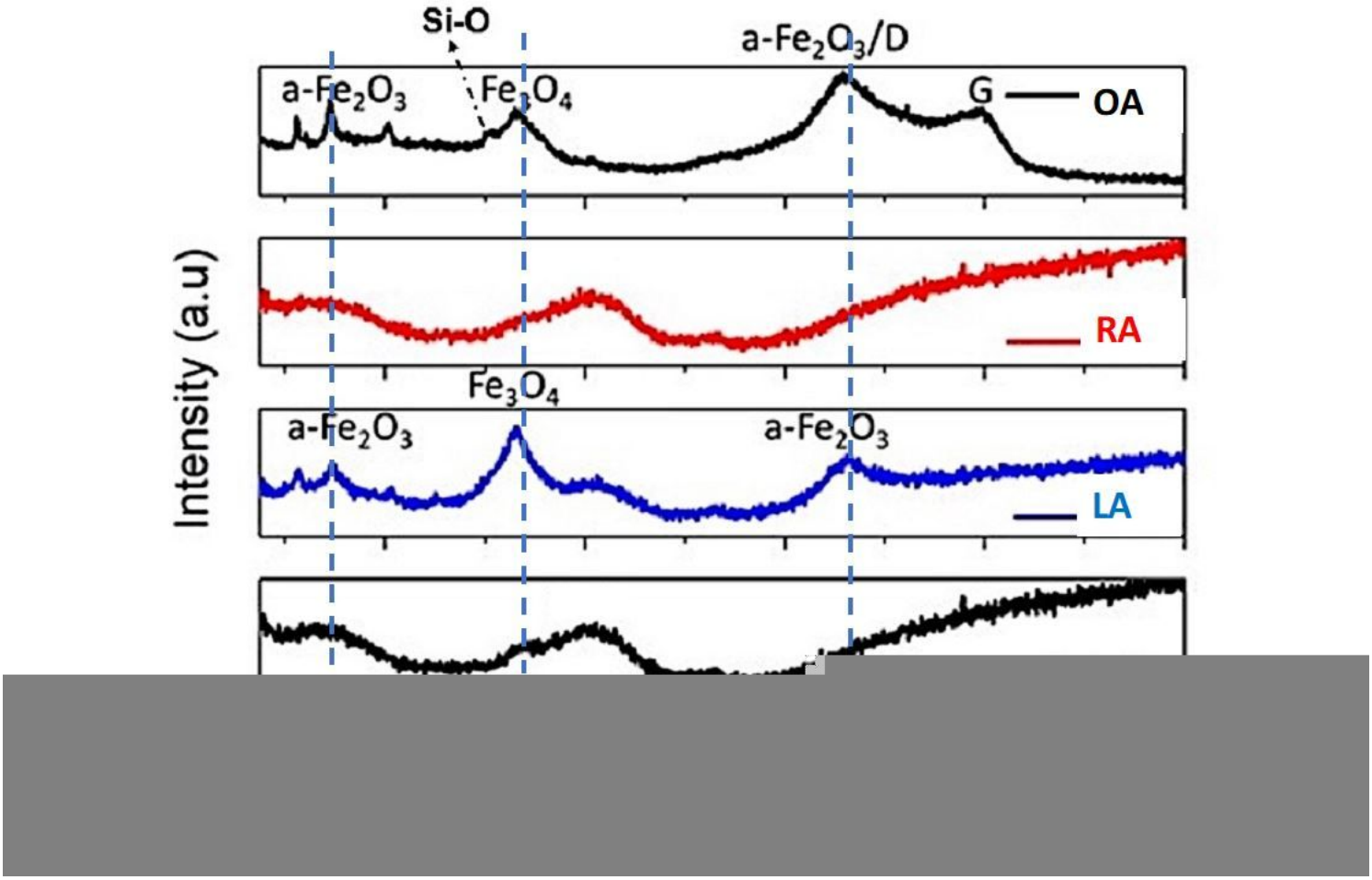

Figure 4

Raman spectra obtained on areas noted in Fig. 2h, j, k. after lubrication by OA, RA, and LA. Analysis of steel pin outside wear scar is also shown.

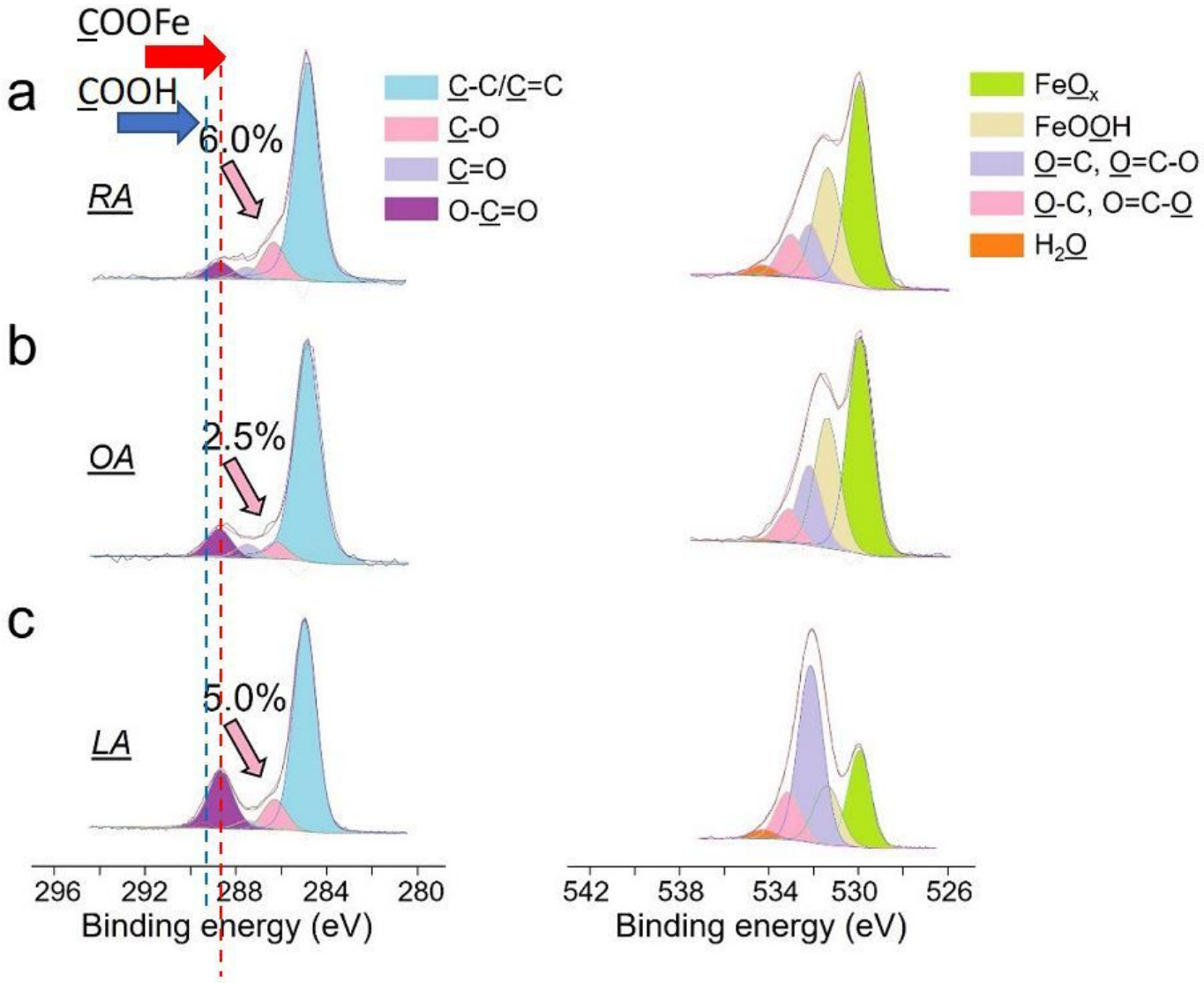

Figure 5

a-c C1s (left side) and O1s (right side) XPS spectra of steel pins after lubrication of **a** OA, **b** RA, and **c** LA. 6.0%, 2.5% and 5.0% in Fig. 5 correspond to C-O content.

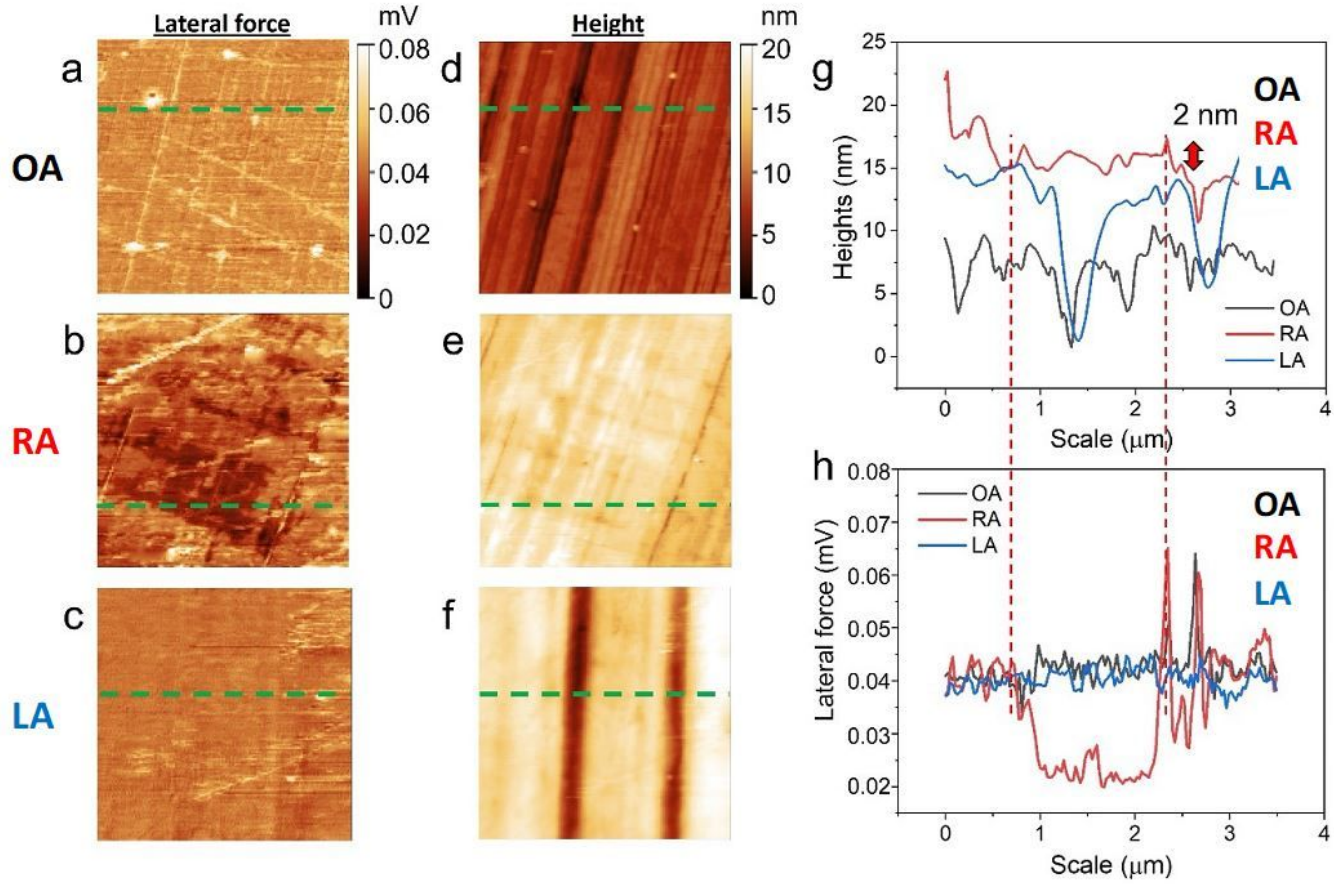

Figure 6

a-f AFM images of steel pins after lubrication by **a**, **d** OA, **b**, **e** RA and **c**, **f** LA, where **d-f** are topographical images and **a-c** lateral force images. **g** height distributions of green lines in d-f. The size analyzed by AFM is 3.5×3.5 mm². **h** lateral force distributions of green lines in a-c.

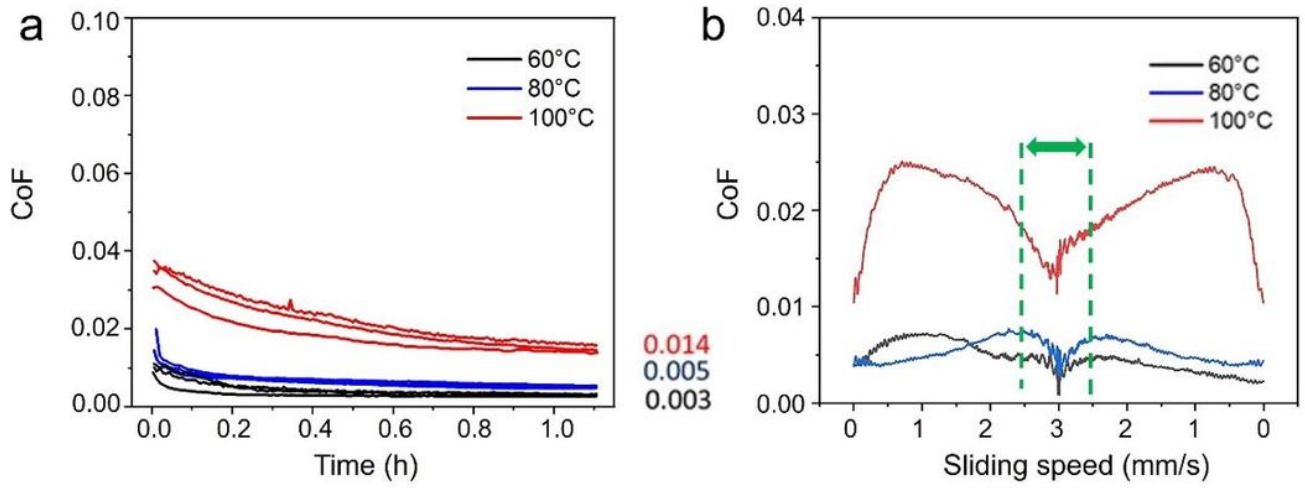

Figure 7

a Correlation between friction and test duration while sliding steel/Si_3N_4 in RA from 60°C to 100°C. The green arrow shows where CoF in Fig.7a is calculated. **b** correlation between CoF and sliding speed was obtained by averaging CoF at each sliding speed of the last 20 cycles.

Supplementary Files

This is a list of supplementary files associated with this preprint. Click to download.

- SIAchievingsuperlubricityofricinoleicacid.docx